A Selective and Sensitive Hg^{2+} Aminonaphthalimide-aza-crown-ether Cellular Chemosensor

Reagan L. Miller,[†] Alena A. Denisenko,[†] Thanh T. Vuong,[†] Austin J. Carlson,[†] Pawan Thapa,[†] Nil K. Pandey,[‡] Wei Chen,[‡] Benjamin J. P. Jones,[‡] and Frank W. Foss Jr*,[†]

†*Department of Chemistry and Biochemistry, University of Texas at Arlington*

‡*Department of Physics, University of Texas at Arlington, Arlington*

E-mail: ffoss@uta.edu

Abstract

Crown ether ionophores linked to napthalimide fluorophores provide a powerful and versatile class of fluorescent chemosensors. Here we demonstrate the unusual Hg^{2+} ion selectivity of an aza-crown ether binding domain and 4-aminonapthalimide fluorophore linked together by electron rich 1,4-phenylenediamine. Binding, computational, and fluorescence studies reveal both photoinduced electron transfer and intramolecular charge transfer mechanisms in operation. The sensor demonstrates exceptional selectivity for Hg^{2+} in aqueous ethanol and detects both Hg^{2+} and Zn^{2+} in aqueous acetonitrile. Mercury ion sensitivity is retained in live cells at biologically relevant concentrations of Hg^{2+}, making it a potentially versatile and convenient tool for environmental and biological assay and monitoring applications.

Introduction

The measurement of heavy metals is critical to the health and sustainability of earth and human systems. Introduced into the atmosphere from natural and anthropomorphic activities, heavy metals persist [1–5] and their bioaccumulation enhance risks to human and environmental health. Mercury has essentially no safe exposure limit, causing significant health risks.[6,7] As recognized by the World Health Organization (WHO) as one of the most toxic metals,[8] mercury causes cancers,[9] and neurological[10] and genetic[11] disorders. With wide distribution in air,[12] water,[13] and soil,[14] mercury must be carefully monitored and regulated. Somewhat overlooked, mercury's caustic nature is also detrimental to industrial equipment.[15,16] Its corrosive presence, when undetected, has led to avoidable economic impact, especially in petroleum refining.[17,18] Therefore, a substantial effort has been made to detect mercury ions, especially CH_3Hg^+ and Hg^{2+} ions.[19]

Beneficial metals like zinc require close monitoring and regulation as well. Zinc is an essential metal needed for proper metabolic reactions, gene and cellular regulation.[20] However, abnormal levels of zinc in the human body can cause complications like diabetes, epilepsy,

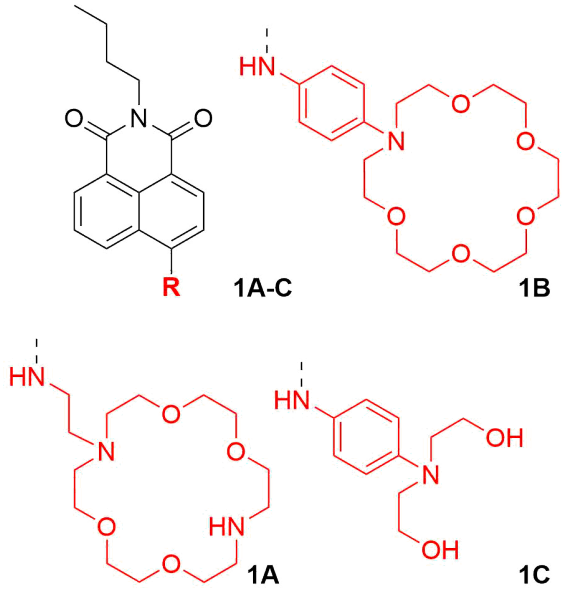

Figure 1: Aminonaphthalimides **1A-1C** with fluorophore in black and binding domains in red.

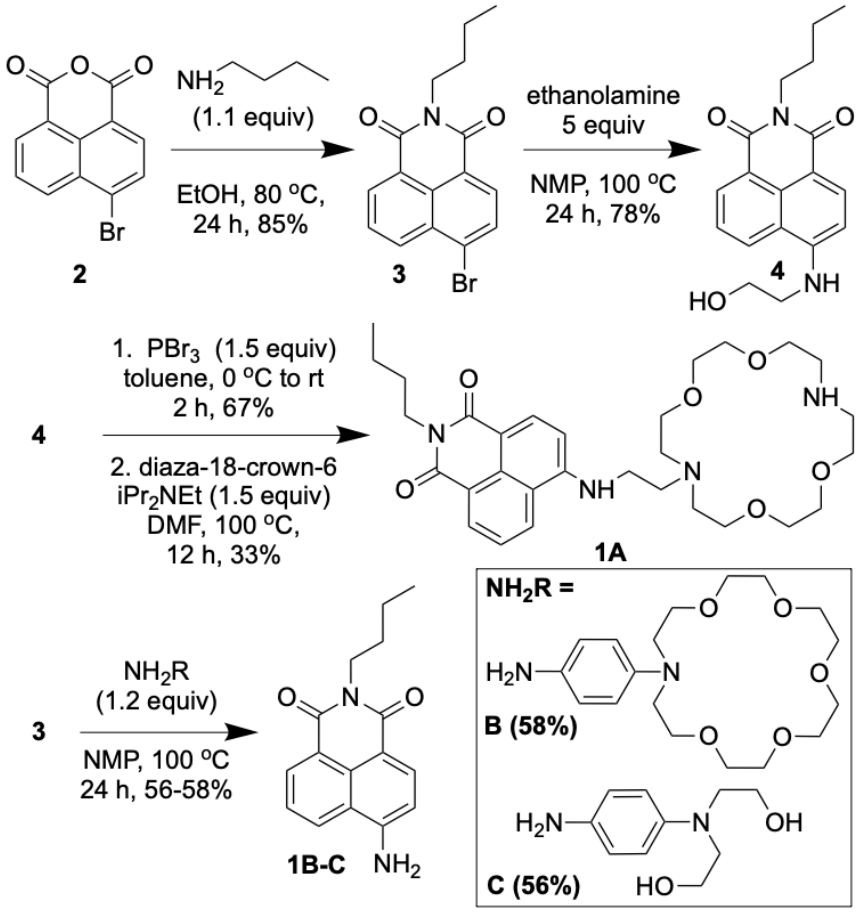

Figure 2: Divergent Synthesis of Aminonaphthalimide Sensors **1A-1C** from common intermediate **3**

and Alzheimer's disease.[21] Therefore, despite their different level of toxicity and environmental and biological impact, mercury and zinc metal/metal ions have been significantly studied using different analytical approaches.

Current analytical techniques for detecting Hg^{2+} and other heavy metal ions rely on sophisticated instrumentation techniques, including inductively coupled plasma mass spectrometry (ICP-MS), atomic emission spectroscopy (ICP-AES), and atomic absorption spectroscopy (AAS). While these methods represent the gold standard in sensitivity, they require costly equipment, training, and sample preparation. Fluorescent techniques are comparatively rapid, sensitive, and cost-effective; coupled with advances in optics, fluorescence mea-

surements can be made at low levels of detection by routine instrumentation. Though currently requiring more advanced microscopy, fluorescence measurements can image even individual ions through single-molecule fluorescence techniques.[22–25] Significant efforts, therefore, exist toward fluorescent sensors of metals, and with the advent of turn-on chemosensors that bind individual ions, the potential for enhanced sensitivity and selectivity is growing.[26–38]

Seeking synthetically tractable fluorescence sensors with new levels of selectivity and sensitivity for heavy metals, we investigated the joining of crown ether ionophores to naphthalimides through conjugated phenylene diamine linkers. Naphthalimide fluorophores have performed well with Hg ion sensors, but few are coupled with azacrownethers without the inclusion of complex connecting functionality.[39–47]

Here we report the design of a Hg^{2+} selective aminonaphthalimide-aza-crown-ether sensor capable of select fluorescence in solution and within living cells, which has significant selectivity for Hg^{2+} ions and therefore potential as a functional chemosensor for trace mercury in various applications (Figure 1). These selective turn-on chemosensors identify Hg^{2+} primarily by an internal charge transfer (ICT) mechanism. We previously demonstrated that this class of molecules[25,48,49] has promise for their function tailored chemical interfaces between gas and solid optical devices for rare event searches in nuclear physics.[24,50–52] In addition to the beneficial properties expected above, we demonstrate a useful binary transition that allows for ultra-sensitive turn-on analysis when taking advantage of a near-threshold turn-on response. This new variant demonstrates selective and sensitive Hg^{2+} detection in whole cells with limited toxicity, potentially providing an immediate tool for sampling heavy metals in cells.

Experimental Section

Materials

Commercially available chemicals were used without further purification unless specified. Spectrophotometric or HPLC-grade acetonitrile was used. Toluene and hexanes were freshly dried and distilled prior to use. Ultrapure water from a Water Pro BT water station was used for ultra-trace analysis.

Equipment

Fluorescence spectra were recorded using a Cary Eclipse Fluorescence Spectrophotometer from Agilent Technologies (Product Number G8800A) at room temperature (25 °C). Instrumental set up: PMT detector voltage-High, Excitation filter-Auto, Emission filter-Open, Excitation slit width-2.5 nm, Emission slit width-5.0 nm, scan control-medium, spectral range 420 nm to 700 nm. All measurements were taken using type 18 quartz microcuvettes with 10 mM path length. Solutions of probe molecules were prepared at 1×10^{-3} M concentration in acetonitrile. Solutions of metal perchlorate salts (Ag^{+}, Ba^{2+}, Ca^{2+}, Cu^{2+}, Cd^{2+}, Cs^{+}, Hg^{2+}, K^{+}, Li^{+}, $N(CH_3)_4^{+}$, Mg^{2+}, Na^{+}, Pb^{2+}, Rb^{+}, Sr^{2+}, Zn^{2+}) were prepared at 1×10^{-2} M concentration in 9:1 acetonitrile/water mixture. All fluorescent studies were done by dilution of the probe molecule to 2×10^{-5} M (20 μM). Metal ion selectivity studies were done by diluting metal perchlorate solutions to 1×10^{-4} M (100 μM) concentration. ^{1}H NMR spectra were recorded on 300 MHz or 500 MHz spectrometers and referenced to the residual solvent signals (7.26 ppm in $CDCl_3$ or 3.33 ppm in CD_3OD). ^{13}C $\{^{1}$H$\}$ NMR spectra were recorded on 75 MHz or 125 MHz spectrometers referenced to the residual solvent signal (77.0 ppm in $CDCl_3$ or 45.0 ppm in CD_3OD). NMR data are reported as follows: chemical shift (δ, ppm), integration (H), multiplicity (s-singlet, d-doublet, t-triplet, q-quartet, m-multiplet, br-broad), coupling constant (J, Hz). High-resolution mass spectrometry (HRMS) data were recorded using a Shimadzu TOF spectrometer in the Shimadzu Center for Advanced Analyt-

ical Chemistry at UT Arlington. Fourier transform- infrared (FT-IR) spectra were recorded using a Bruker Alpha-P FT-IR spectrophotometer by attenuated total reflectance on a diamond sample plate. Thin-layer chromatography was performed on silica gel-coated aluminum plates (EMD Merck F254, 250 μm thickness). Flash chromatography was performed over Silicycle Silicafash P60 silica gel (mesh 230–400) or standard-grade activated Alumina (mesh 50–300). Melting points were recorded in capillary tubes on a Mel-Temp II apparatus and were uncorrected.

Results and Discussion

Synthesis

The preparation of probes **1A-1C** (Figure 2) was completed by condensation of commercially available butylamine with bromonaphthalic anhydride **2** to produce common naphthalimide intermediate **3**. Aryl bromide **3** was diversified into compounds **1A-1C** by nucleophilic aromatic substitution with ethanolamine to give **4**, or with independently prepared anilines to yield **1B** and **1C** directly. Compound **4** was further elaborated by PBr_3 bromination and nucleophilic substitution with 1,10-diaza-18-crown-6-ether to provide **1A**.

UV-Vis absorption studies

All fluorescent probes were initially measured in acetonitrile solution to determine their photophysical properties. The absorption spectra of all probes, shown in Figure 3 (left), appear to have broad peaks around 200-300 nm, and 350-500 nm, which are consistent with the 1,8-naphthalimide chromophore. Probe **1B** and **1C** showed a red-shifted λ_{max} around 450 nm compared to probe **1A** (λ_{max} ~430 nm) due to an extended aniline chromophore. The optical response of sensor **1B**, when exposed to different metal cations, was studied with UV/Vis and fluorescence spectroscopy. In acetontrile, the addition of mercury and zinc perchlorate solution led to a shift of the absorption maximum from 450 nm to 430 nm,

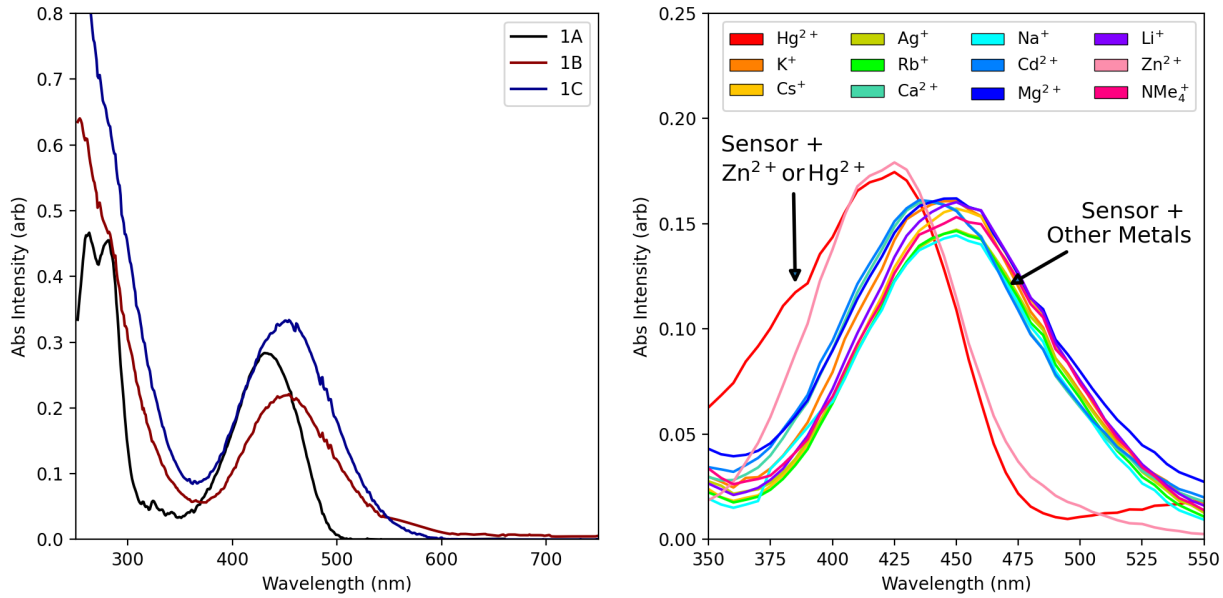

Figure 3: Left: UV-Vis absorption spectra of probe **1A**-**1C** (25 μM) in acetonitrile at room temperature. Right: UV-Vis absorption spectra of **1B** (20 μM) in acetonitrile with and without 5 equiv. of metal/nonmetal perchlorate in 9:1 acetonitrile/HEPES buffer at room temperature.

followed by a visible color change from red to yellow in the case of probe **1B**, while the addition of equivalent amounts of most other metal ions resulted in no change in absorption maxima or corresponding observations of color change (Figure 3, right). This suggests that it follows the intramolecular charge transfer (ICT) mechanism.

Different solvents were investigated in order to see how they would alter the selectivity (Figure 4, left). During the measurements, the λ_{max} value shifted to 460 nm, with DCM exhibiting a change in color from red to pink, and the shift of the λ_{max} value to 510 nm due to the low polarity and low viscosity of the solvent, since non-polar solvents are not affected by the dipole effect of the fluorophore. Ethanol was used as a solvent for testing the response to metal perchlorates that had the effect of losing their vibrational fine structure due to their high polarity and increased viscosity compared to methanol. A shift of the maximum absorption wavelength was observed as Hg^{2+} was added, moving from 460 nm to 440 nm, followed by a visible change from red to yellow, while lead and other metals did not show any significantly different behavior (Figure 4, right). Adding zinc perchlorate did

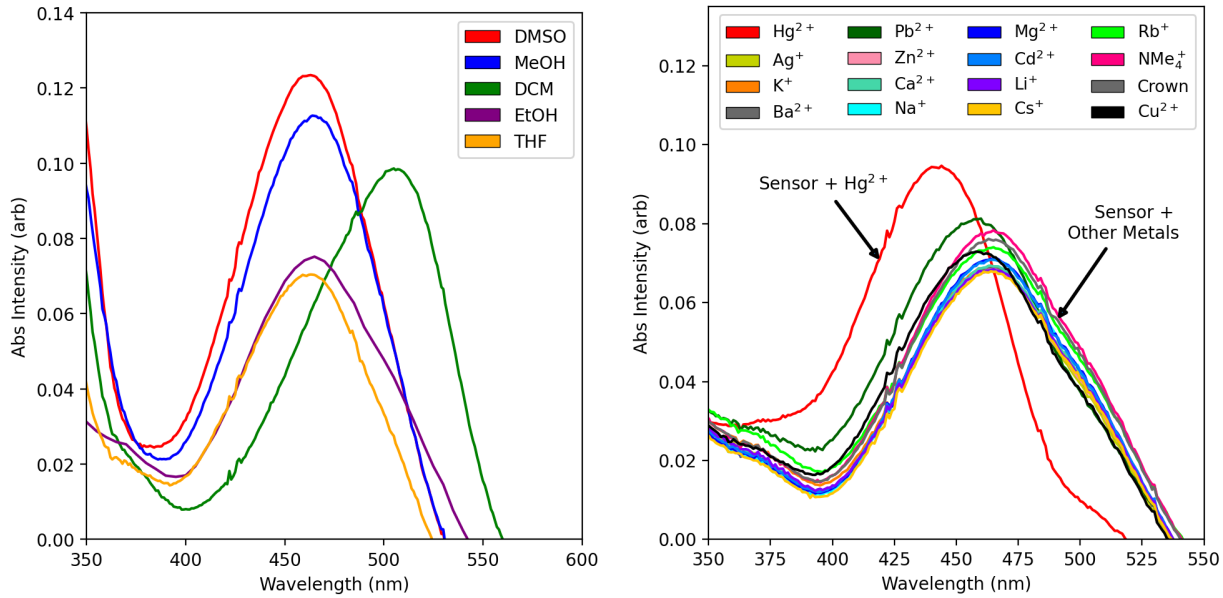

Figure 4: Left: UV-Vis absorption spectra of probe **1B** (25 μM) in various solvents at room temperature. Right: UV-Vis absorption spectra of probe **1B** (20 μM) in ethanol in the presence of 5 equiv. of various metal/nonmetal perchlorates at room temperature.

not result in a change to the absorption, leading to the conclusion that ethanol was the best solvent for Hg^{2+} selectivity.

Fluorescence spectroscopic studies

Fluorescent probe **1B** shows an extremely strong response to added Hg^{2+} at the tens-of-μM level in ethanol. Two-dimensional emission/excitation spectra for the unbound and Hg^{2+}-bound sensor at 20 μM in ethanol with 15 μM mercury perchlorate salt added are shown in Figure 5, left. A photograph showing the visible fluorescent emission of the bound and unbound solutions under 405 nm excitation is shown in Fig. 5, right. In all subsequent fluorescence studies reported, the mixture is excited at 430 nm.

We tested fluorescent response of probe **1B** against various metal/nonmetal perchlorates. To evaluate the sensitivity and selectivity of **1B** toward Hg^{2+}, a competition experiment (Figure 6) was performed. A number of different metal/nonmetal ions were used to test the complexation ability of the receptor, including Ag^{+}, Ba^{2+}, Ca^{2+}, Cu^{2+}, Cd^{2+}, Cs^{2+},

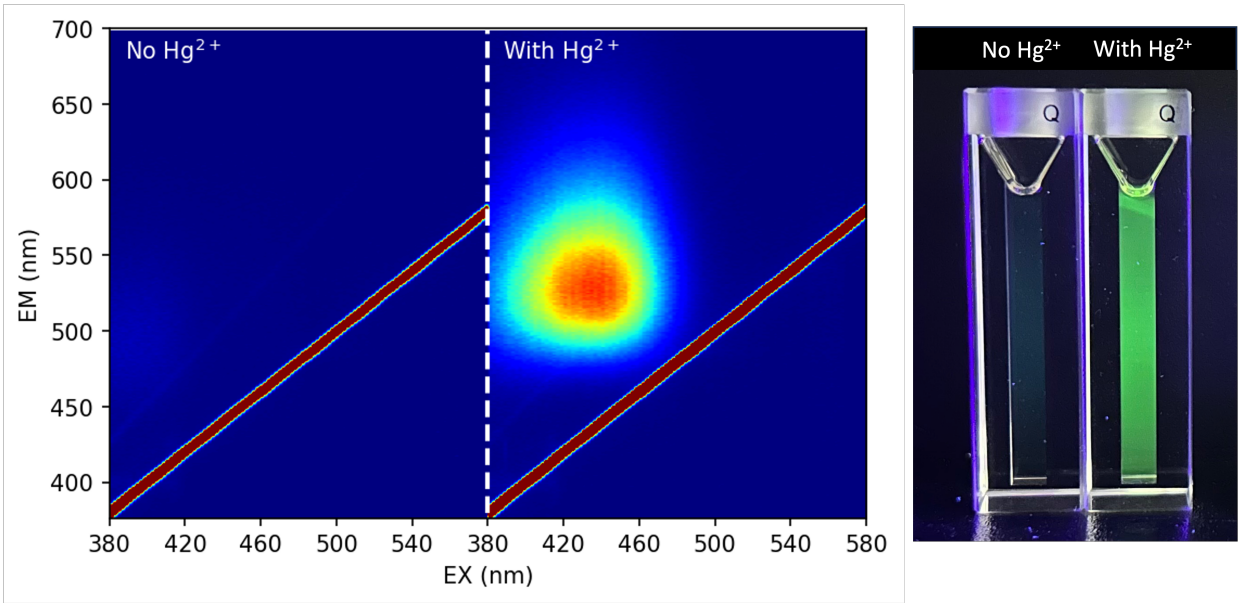

Figure 5: Left: 3D emission-excitation spectrum for the unbound (left) and Hg^{2+}-bound (right) mercury sensor **1B** in ethanol, Right: photograph of fluorescence in unbound (left) and Hg^{2+}-bound (right) mercury sensor.

Hg^{2+}, K^{+}, Li^{+}, $N(CH3)_3^{+}$, Mg^{2+}, Na^{+}, Pb^{2+}, Rb^{2+}, Sr^{2+}, and Zn^{2+}. We maintained the concentration of the solution of the molecule probe in ethanol at 10 μM with the addition of 5 equivalence of metal/nonmetal perchlorates. In all cases, a one minute incubation in the dark was allowed before taking measurements. Strong selectivity and sensitivity to Hg^{2+} is observed, and this sensitivity is unimpaired by admixture of other ions into the solution.

Fluorescence studies were performed first in acetonitrile followed by ethanol to probe the effect of changing solvents on the emission of **1B**. At all concentrations in both solvent systems, **1B** is pale orange and does not emit fluorescent signal. In acetonitrile, the addition of Hg^{2+} and Zn^{2+} at various concentrations results in a color change from pale orange to yellow along with fluorescence emission with peak excitation at 430 nm. This intensity gradually increases (Figure 7) from a low intensity with the addition of metal perchlorates to the maximum intensity with the addition of 0.04 mM Hg^{2+} and 0.10 mM Zn^{2+}. In ethanol, only the addition of Hg^{2+} at varying concentrations results in the color change from pale orange to yellow along with fluorescent emission. This intensity increases (Figure 8) to a maximum intensity with the addition of 0.03 mM of Hg^{2+}. As shown in Job's plot analysis

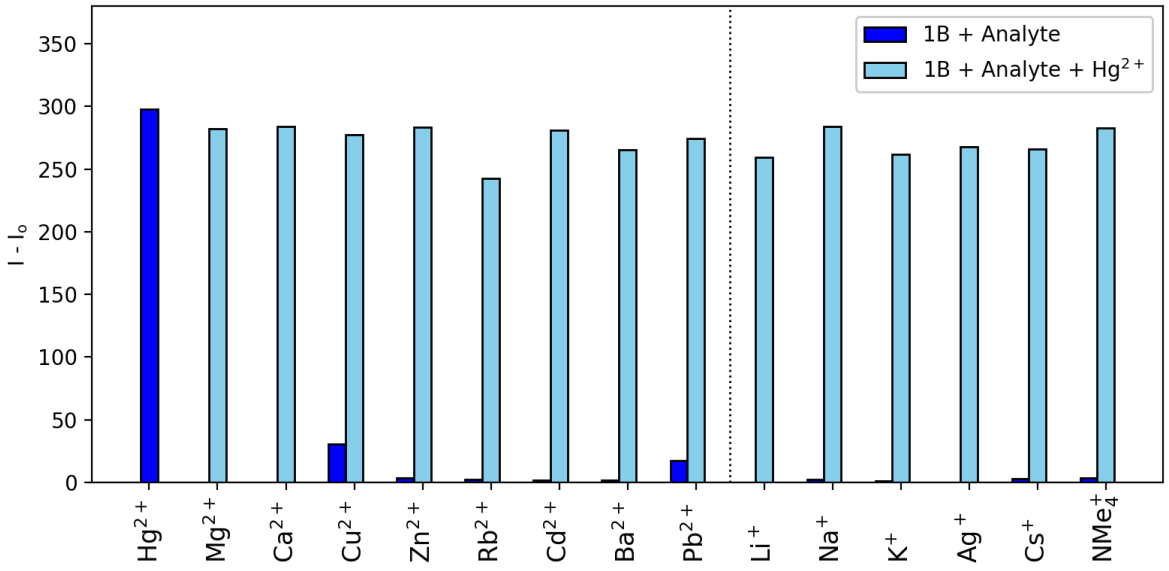

Figure 6: Competitive fluorescence response of **1B** (10 μM) to Hg^{2+}(50 μM) in the presence of other metal/nonmetal ions (ions, 50 μM) in 8:2 ethanol/water. Excited at λ_{ex} 430 nm.

the ligands bound in ethanol with a stoichiometric 1:1 complex with Hg^{2+} perchlorate in a 9:1 acetonitrile/HEPES buffer stock solution (Figure 9).

This sensing system displays a notable non-linearity in fluorescence response at low Hg^{2+} concentrations. Up to a threshold value of 8 μM no fluorescence is induced, and above this limit a rapid switch-on behaviour is observed. We have observed this non-linearity observed in multiple solvents and instrument settings, and also validated it via US-Vis absorption spectroscopy. We speculate that is caused by the partial dissociation of the perchlorate salt at low concentrations to $[HgClO_4]^+$ and Cl^-, with production of the dication Hg^{2+} becoming substantial at higher concentrations. The complex and concentration-dependent speciation of dicationic salts is well documented.[53–56] To test this hypothesis a comparison was made to $HgCl_2$ salt which is well known to dissociate weakly, and then predominantly to $[HgCl]^+$ and Cl^- at all relevant concentrations studied[2,57,58] . In the latter case no fluorescence was observed at any concentration despite the ready solubility of the $HgCl_2$ in both solvent systems, supporting the hypothesis of ion speciation dependence of fluorescence. This nonlinear response may appear to impose a modest limit of detection for dissolved Hg, but it also of-

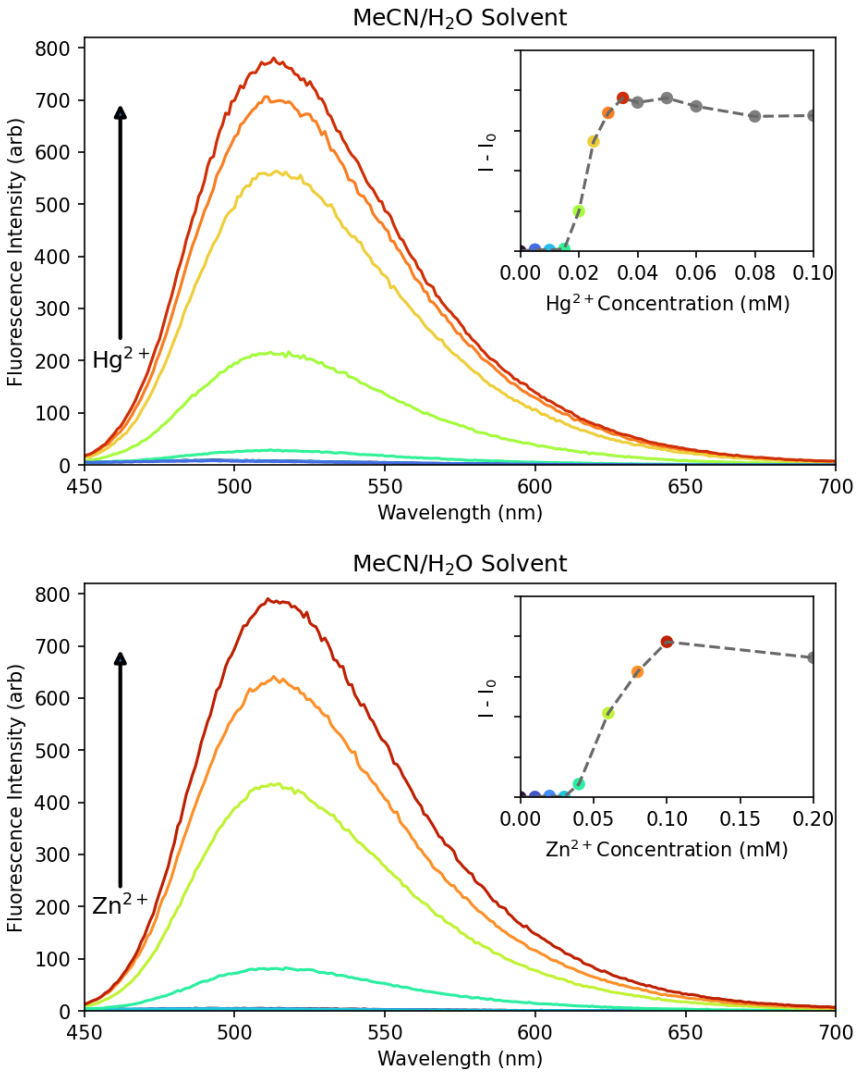

Figure 7: Top: Titration fluorescence spectra of **1B** (20 μM) in acetonitrile with Hg^{2+} perchlorate in 9:1 acetontrile/HEPES buffer stock solution at λ_{max} 430 nm. Bottom: Titration fluorescence spectra of **1B** (20 μM) in acetonitrile with Zn^{2+} perchlorate in 9:1 acetontrile/HEPES buffer stock solution at λ_{max} 430 nm.

fers an opportunity for a dramatically enhanced limit of detection using pre-spiked solutions prepared at the transition edge. Because the local gradient of fluorescence vs concentration is substantially increased near threshold, world-leading limits of detection of 1.44 nM (using the standard protocol of gradient / noise floor 3σ[59]) are obtained if the starting solution is prepared to sit at the transition point. This approach resembles the exploitation of nonlinear phenomena employed elsewhere in precision sensing, for example, transition edge sensors

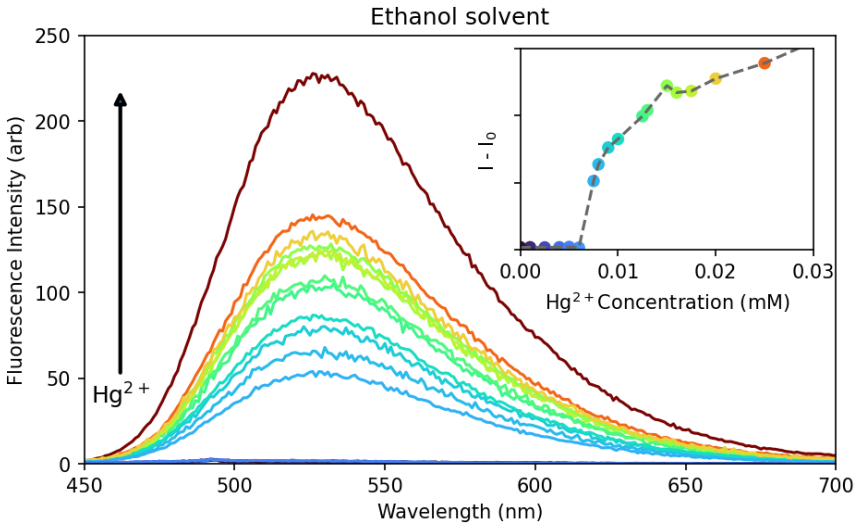

Figure 8: Titration fluorescence spectra of **1B** (20 μM) in ethanol with Hg^{2+} perchlorate in 9:1 acetonitrile/water at λ_{ex} 430 nm.

based on materials held at the threshold of superconductive phase transitions presently represent the worlds most sensitive known bolometers.[60,61] To our knowledge, exploitation of fluorescent sensing systems with nonlinear near-threshold response to enhance limit of detection has not been previously reported as an ion assay method. Such systems appear to offer highly promising approaches to ultra-precise metal assay through fluorescence.

^{1}H NMR studies

1B was further analyzed through ^{1}H NMR experiments. The initial attempt to study the effect of Hg^{2+} on sensor **1B** in acetonitrile-d3 solution was not successful due to precipitation of an unknown dark brown solid as well as a significant peak broadening effect. However, the precipitation issue was resolved with the use of CD_3Cl solvent in the case of mercury salt. When mercury and zinc perchlorate salts were added in five equivalents separately to the CD_3Cl and CD_3CN solution respectively containing 14 mM of sensor **1B**, we observed a significant deshielding effect in protons of both phenyl substituent (H7-H10) and naphthalimide ring (H2-H6) concomitant to visual color change from red to yellowish-brown. Crown ether protons were found to have the mixed effect of shielding and deshielding, presumably due to

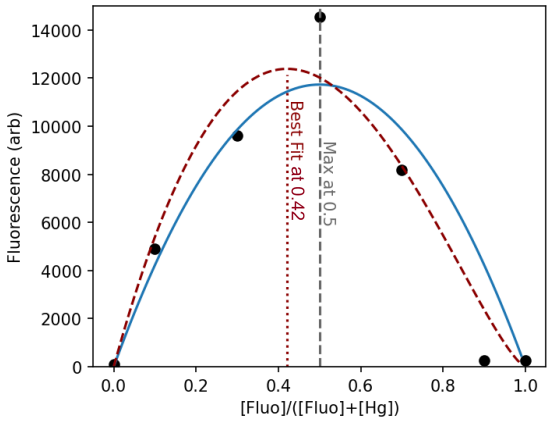

Figure 9: Jobs plot analysis of Hg^{2+} binding to **1B**, suggesting a 1:1 stoichiometry, as predicted by simulations.

the reorganization of the crown ring upon binding to Hg^{2+} or Zn^{2+} ions (Figure 10). These preliminary investigations through NMR studies strongly indicate complexation of Hg^{2+} and Zn^{2+} ions with both nitrogen of the phenyl group, thereby affecting intramolecular charge transfer from nitrogen substituents to carboxyimide group in naphthalimide fluorophore; the effect which was further supported by UV-Vis result.

Computational Evaluation

The optimization and frequency of probe **1B** without (left) and with (right) Hg^{2+} Figure 11 was performed by computational studies, carried out using the Gaussian 09 program.[62] A polymerizable continuum model (PCM)[63] and m062x density functional[64] were used to calculate the species in acetonitrile solution with the def2svp basis set.[65,66] A Multiwfn analyzer and Gaussview were used to determine the visible orbital geometry of the molecule.

The mechanism for fluorescence switching is illustrated by these calculations as a combination of two clear effects. In the case of the unbound sensor, the dominant excitation mode is from HOMO-1 to LUMO with transition strength 0.70 (green, left), but emission by fluorescence is prohibited by photoinduced electron transfer (PET) from the intermediate HOMO level to the now singly occupied HOMO-1 level of the excited state (orange). Upon binding Hg^{2+}, intramolecular charge transfer (ICT) takes place to shift charge density in the

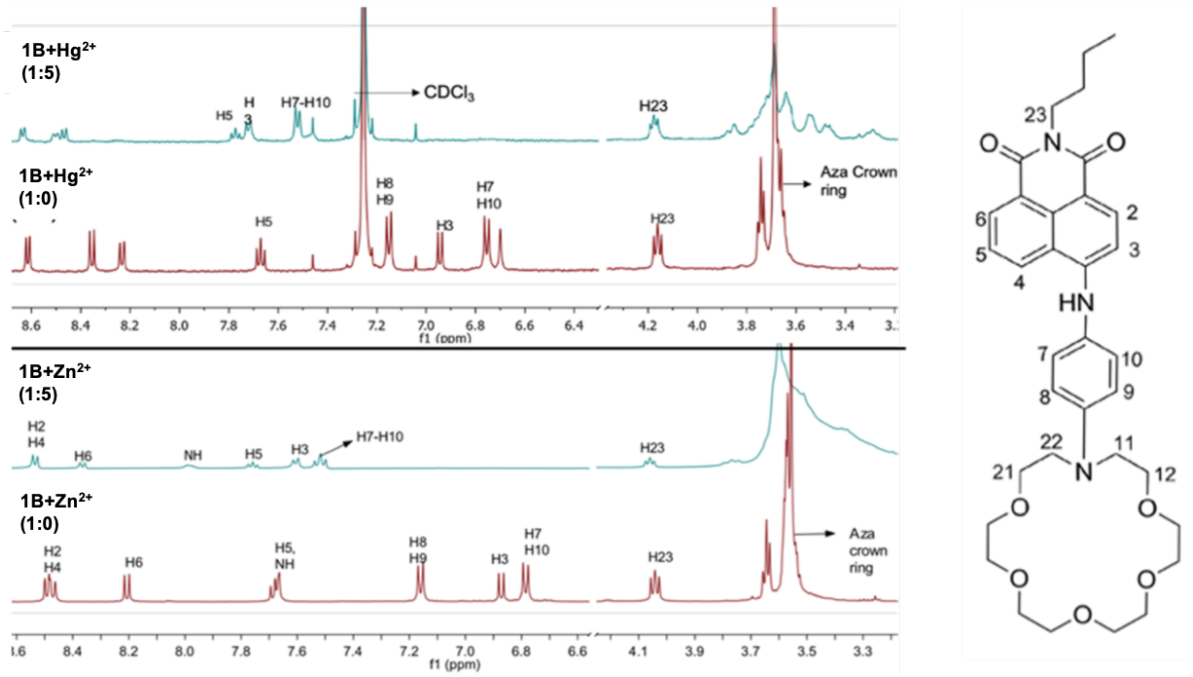

Figure 10: ^{1}H NMR spectra showing the downfield shift of H7-H10 in response to ion chelation, which correlates to the absorption shift by ICT.

HOMO level toward the fluorescent group (cyan); this alters the excitation dynamics such that the excitation transition is now predominantly from HOMO to LUMO+1 (green, right). PET cannot occur following such a transition, so fluorescence is enabled upon ion chelation.

This mechanism is notably somewhat different to the one we have observed in similar species developed for Ba^{2+} sensing,[25] where it is primarily the 're-ordering' of the frontier molecular orbitals upon ion binding rather than evolution of their charge distribution through ICT that is responsible for the PET-induced fluorescence switching behaviour. Combined, the off state of **1B** at the wavelength of excitation to detect Hg^{2+} is extraordinarily dark without the metal analyte.

Biological Studies

The practical application of Hg^{2+} selective probe **1B** was carried out using a fluorescence imaging study for the sensing of Hg^{2+} ions in living cancer cells. To image the cells through sensing of Hg^{2+} ions with probe **1B**, two different concentrations of the probe (50 μM, Figure

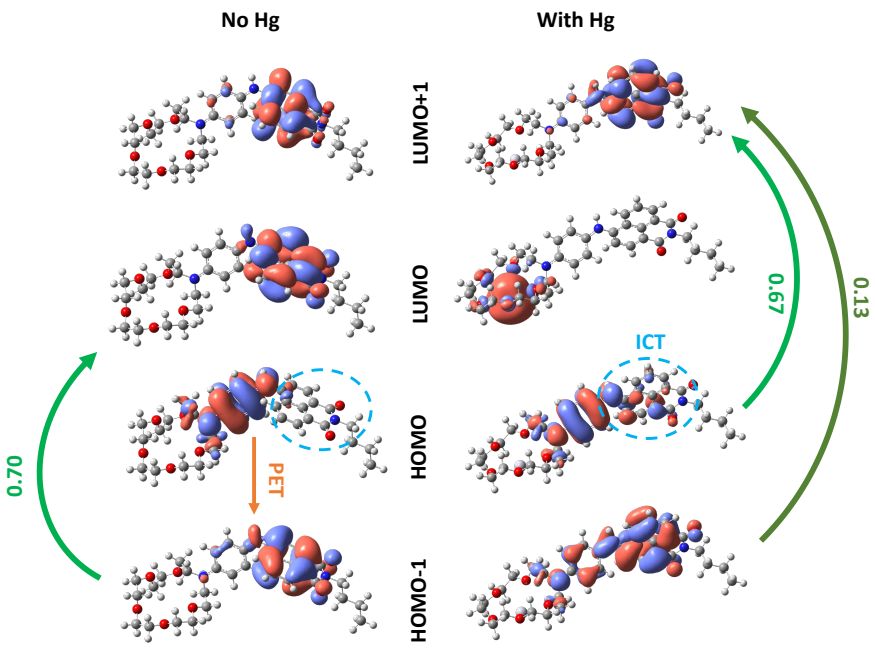

Figure 11: Simulated orbitals of **1B**. Hg^{2+} induced ICT mechanism is illustrated by the metal centered charge density and stabilization of the HOMO level in excess of LUMO and LUMO+1 level stabilization. Bottom: Predicted shift to higher energy absorbance.

12 and 10 μM, see SI) in acetonitrile solution were chosen. In the absence of Hg^{2+} ions, cells treated with the only probe were non-fluorescent. Notably, the cells pretreated with 50 μM of Hg^{2+} ions followed by addition of 50 μM and 10 μM probe **1B** separately in two set of experiments gave bright green fluorescence. Additional representation of overlay images of fluorescence and bright field clearly demonstrates the ability of probe **1B** to cross cell barriers for sensing Hg^{2+} ions in the cytoplasmic level of the cells.

Initially, an MTT assay was performed to examine the toxicity level of the probe **1B** in MCF-7 breast cancer cells. This showed that the probe is almost non-toxic at a wide range of selected concentrations (0.195 - 100 μM) and is suitable to image cells even at high concentrations of the probe (not shown). The cytotoxicity of **1B** against HeLa cells was then evaluated using the MTT assay. The cells were exposed to the sample in the concentration range of 0.20 to 100 μM for 24 h. HeLa cells exhibited good cell viability in the presence of the probe, indicating that **1B** exerts low cytotoxicity in the concentration range of 0.20–100 μM

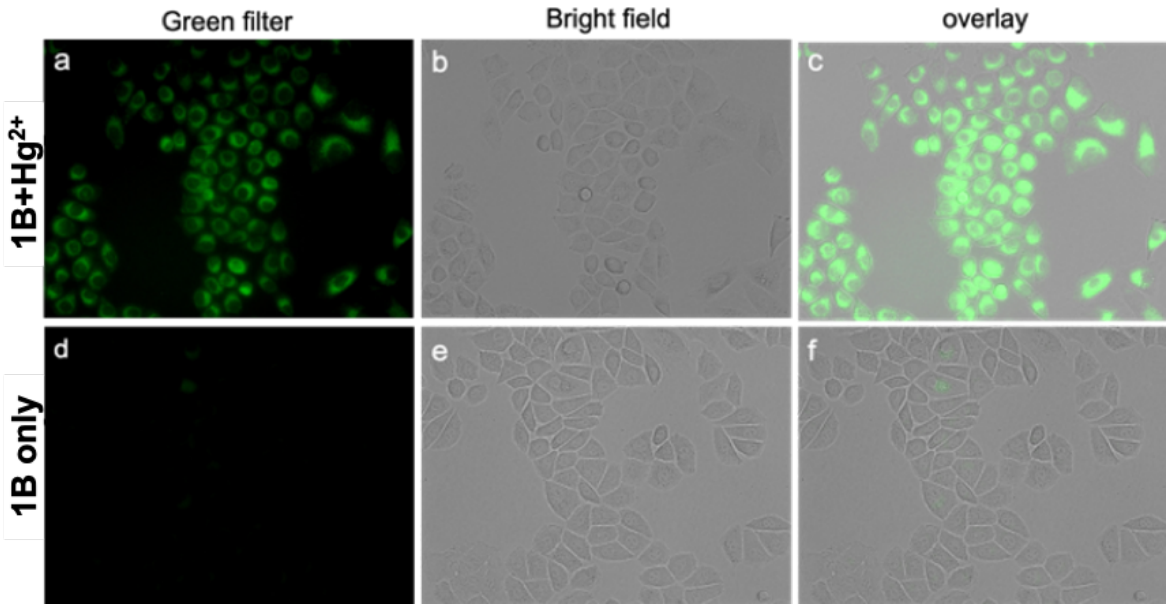

Figure 12: Confocal fluorescence images for the detection of the probe **1B** (50 μM) in the presence (**1B**+Hg^{2+}; a, b, and c) of Hg^{2+} ions (50 μM) and in the absence (**1B** only; d, e, and f) of Hg^{2+} ions. Image a and d are fluorescence images of **1B** and **1B**+Hg^{2+} when excited at 488 nm. Image b and e are corresponding bright-field images of fluorescence images a and d respectively. images c and f are overlay images of both fluorescence and bright field images of a and d respectively.

(see SI). These findings highlight the potential of **1B** in Hg^{2+} detection *in situ* in biological systems.

Conclusion

We have reported the development and synthesis of a selective and sensitive aminonaphthalimide-aza-crown-ether-based ion sensor with a high degree of selectivity for Hg^{2+} in ethanol and Hg^{2+} and Zn^{2+} in acetonitrile/water solvent. Computational and fluorescence studies showed that an intramolecular charge transfer mechanism is predominant in the fluorescence switching process, and the stoichiometry of the binding has been validated to be 1:1 on capture of Hg^{2+}. The maximally sensitive method of mercury assay using this molecule was realized by pre-spiking the sensing mixture with mercury salts to the fluorescence switching transition edge. With such a mixture, world leading limits of detection of 1.5 nM have been

realized. The sensor is rather non-toxic, with MTT assay performed to examine the toxicity level in MCF-7 breast cancer cells, and functions well inside living cells. This molecule thus shows great promise as a convenient probe for toxic Hg^{2+} in environmental and biological applications.

Acknowledgements

This program of toxic metal sensor development was inspired by our ongoing collaborative project to develop SMFI chemosensors functional at the solid-gas interface, as R&D toward barium tagging for the NEXT experiment. Specifically, we thank JJ Gomez Cadenas and Zoraidia Freixa for enlightening conversations and suggestions. We gratefully acknowledge support from the US National Science Foundation under award number NSF CHE 2004111 and the Robert A Welch Foundation under award number Y-2031-20200401 (University of Texas Arlington) the US Department of Energy under awards DE-SC0019054 and DE-SC0019223.

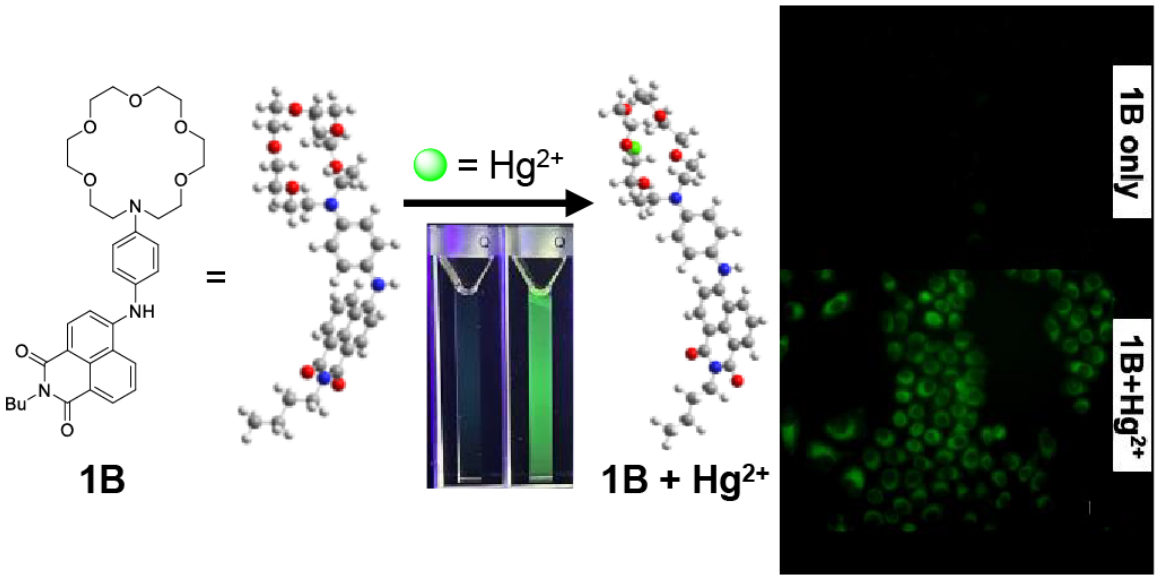

Figure 13: For Table of Contents Only

Graphical Abstract

References

(1) Tomiyasu, T.; Okada, M.; Imura, R.; Sakamoto, H. Vertical variations in the concentration of mercury in soils around Sakurajima Volcano, Southern Kyushu, Japan. *Science of the total environment* **2003**, *304*, 221–230.

(2) Schecher, W. D.; McAvoy, D. C. *MINEQL+: A Chemical Equilibrium Modeling System; Version 4.5 for Windows User's Manual*; Environmental Research Software, 2003.

(3) Sheu, G.-R.; Mason, R. P. An examination of methods for the measurements of reactive gaseous mercury in the atmosphere. *Environmental science & technology* **2001**, *35*, 1209–1216.

(4) Thorneloe, S. A.; Kosson, D. S.; Sanchez, F.; Garrabrants, A. C.; Helms, G. Evaluating the fate of metals in air pollution control residues from coal-fired power plants. 2010.

(5) Tchounwou, P. B.; Yedjou, C. G.; Patlolla, A. K.; Sutton, D. J. Heavy metal toxicity and the environment. *Molecular, clinical and environmental toxicology: volume 3: environmental toxicology* **2012**, 133–164.

(6) Tchounwou, P. B.; Ayensu, W. K.; Ninashvili, N.; Sutton, D. Environmental exposure to mercury and its toxicopathologic implications for public health. *Environmental Toxicology: An International Journal* **2003**, *18*, 149–175.

(7) Nolan, E. M.; Lippard, S. J. Tools and tactics for the optical detection of mercuric ion. *Chemical reviews* **2008**, *108*, 3443–3480.

(8) Organization, W. H., et al. *Inorganic mercury*; World Health Organization, 1991.

(9) Kim, H.; Lee, J.; Woo, H. D.; Kim, D. W.; Oh, J. H.; Chang, H. J.; Sohn, D. K.; Shin, A.; Kim, J. Dietary mercury intake and colorectal cancer risk: A case-control study. *Clinical Nutrition* **2020**, *39*, 2106–2113.

(10) Albers, J. W.; Kallenbach, L. R.; Fine, L. J.; Langolf, G. D.; Wolfe, R. A.; Donofrio, P. D.; Alessi, A. G.; Stolp-Smith, K. A.; Bromberg, M. B.; Group, M. W. S. Neurological abnormalities associated with remote occupational elemental mercury exposure. *Annals of neurology* **1988**, *24*, 651–659.

(11) Haley, B. E. Mercury toxicity: genetic susceptibility and synergistic effects. *Medical Veritas* **2005**, *2*, 535–42.

(12) Cole, A. S.; Steffen, A.; Eckley, C. S.; Narayan, J.; Pilote, M.; Tordon, R.; Graydon, J. A.; St. Louis, V. L.; Xu, X.; Branfireun, B. A. A survey of mercury in air and precipitation across Canada: patterns and trends. *Atmosphere* **2014**, *5*, 635–668.

(13) Kallithrakas-Kontos, N.; Foteinis, S. Recent advances in the analysis of mercury in water-review. *Current Analytical Chemistry* **2016**, *12*, 22–36.

(14) Xu, J.; Bravo, A. G.; Lagerkvist, A.; Bertilsson, S.; Sjöblom, R.; Kumpiene, J. Sources and remediation techniques for mercury contaminated soil. *Environment international* **2015**, *74*, 42–53.

(15) Finster, M. E.; Raymond, M. R.; Scofield, M. A.; Smith, K. P. Mercury-impacted scrap metal: Source and nature of the mercury. *Journal of Environmental Management* **2015**, *161*, 303–308.

(16) Abbasa, T.; Nazir, S.; Øvergårdb, K. I.; Mancac, D.; Abdul, M. Hazards of mercury–safety perspectives and measures. *Chemical Engineering* **2015**, *43*.

(17) Wilhelm, S. M.; Bloom, N. Mercury in petroleum. *Fuel Processing Technology* **2000**, *63*, 1–27.

(18) Mojammal, A.; Back, S.-K.; Seo, Y.-C.; Kim, J.-H. Mass balance and behavior of mercury in oil refinery facilities. *Atmospheric Pollution Research* **2019**, *10*, 145–151.

(19) Oh, S.; Jeon, J.; Jeong, J.; Park, J.; Oh, E.-T.; Park, H. J.; Lee, K.-H. Fluorescent detection of methyl mercury in aqueous solution and live cells using fluorescent probe and micelle systems. *Analytical chemistry* **2020**, *92*, 4917–4925.

(20) Maret, W.; Sandstead, H. H. Zinc requirements and the risks and benefits of zinc supplementation. *Journal of trace elements in medicine and biology* **2006**, *20*, 3–18.

(21) Zhang, Y.; Xiao, J.-Y.; Zhu, Y.; Tian, L.-J.; Wang, W.-K.; Zhu, T.-T.; Li, W.-W.; Yu, H.-Q. Fluorescence sensor based on biosynthetic CdSe/CdS quantum dots and liposome carrier signal amplification for mercury detection. *Analytical chemistry* **2020**, *92*, 3990–3997.

(22) Bagh, S.; Paige, M. F. Ensemble and single-molecule fluorescence spectroscopy of a calcium-ion indicator dye. *The Journal of Physical Chemistry A* **2006**, *110*, 7057–7066.

(23) Harms, G. S.; Cognet, L.; Lommerse, P. H.; Blab, G. A.; Kahr, H.; Gamsjäger, R.; Spaink, H. P.; Soldatov, N. M.; Romanin, C.; Schmidt, T. Single-molecule imaging of L-type Ca2+ channels in live cells. *Biophysical Journal* **2001**, *81*, 2639–2646.

(24) McDonald, A.; Jones, B.; Nygren, D.; Adams, C.; Álvarez, V.; Azevedo, C.; Benlloch-Rodríguez, J.; Borges, F.; Botas, A.; Cárcel, S., et al. Demonstration of single-barium-ion sensitivity for neutrinoless double-beta decay using single-molecule fluorescence imaging. *Physical review letters* **2018**, *120*, 132504.

(25) Thapa, P.; Byrnes, N. K.; Denisenko, A. A.; Mao, J. X.; McDonald, A. D.; Newhouse, C. A.; Vuong, T. T.; Woodruff, K.; Nam, K.; Nygren, D. R., et al. Demonstration of selective single-barium ion detection with dry diazacrown ether naphthalimide turn-on chemosensors. *ACS sensors* **2021**, *6*, 192–202.

(26) Chasapis, C. T.; Loutsidou, A. C.; Spiliopoulou, C. A.; Stefanidou, M. E. Zinc and human health: an update. *Archives of toxicology* **2012**, *86*, 521–534.

(27) Cui, W.-R.; Zhang, C.-R.; Jiang, W.; Liang, R.-P.; Wen, S.-H.; Peng, D.; Qiu, J.-D. Covalent organic framework nanosheet-based ultrasensitive and selective colorimetric sensor for trace Hg2+ detection. *ACS Sustainable Chemistry & Engineering* **2019**, *7*, 9408–9415.

(28) Xiaoxiong, Z.; Wenjun, Z.; Cuiliu, L.; Xiaohong, Q.; Chengyu, Z. Eu3+-postdoped UIO-66-type metal–organic framework as a luminescent sensor for Hg2+ detection in aqueous media. *Inorganic Chemistry* **2019**, *58*, 3910–3915.

(29) Malek, A.; Bera, K.; Biswas, S.; Perumal, G.; Das, A. K.; Doble, M.; Thomas, T.; Prasad, E. Development of a next-generation fluorescent turn-on sensor to simultaneously detect and detoxify mercury in living samples. *Analytical chemistry* **2019**, *91*, 3533–3538.

(30) Chatterjee, A.; Banerjee, M.; Khandare, D. G.; Gawas, R. U.; Mascarenhas, S. C.; Ganguly, A.; Gupta, R.; Joshi, H. Aggregation-induced emission-based chemodosimeter approach for selective sensing and imaging of Hg (II) and methylmercury species. *Analytical chemistry* **2017**, *89*, 12698–12704.

(31) Shaily,; Kumar, A.; Ahmed, N. Indirect approach for CN–detection: development of "naked-eye" Hg2+-induced turn-off fluorescence and turn-on cyanide sensing by the Hg2+ displacement approach. *Industrial & Engineering Chemistry Research* **2017**, *56*, 6358–6368.

(32) Zhang, S.; Zhang, D.; Zhang, X.; Shang, D.; Xue, Z.; Shan, D.; Lu, X. Ultratrace naked-eye colorimetric detection of Hg2+ in wastewater and serum utilizing mercury-stimulated peroxidase mimetic activity of reduced graphene oxide-PEI-Pd nanohybrids. *Analytical chemistry* **2017**, *89*, 3538–3544.

(33) Ge, Y.; Liu, A.; Ji, R.; Shen, S.; Cao, X. Detection of Hg2+ by a FRET ratiometric

fluorescent probe based on a novel pyrido [1, 2-a] benzimidazole-rhodamine system. *Sensors and Actuators B: Chemical* **2017**, *251*, 410–415.

(34) Ge, Y.; Xing, X.; Liu, A.; Ji, R.; Shen, S.; Cao, X. A novel imidazo [1, 5-a] pyridine-rhodamine FRET system as an efficient ratiometric fluorescent probe for Hg2+ in living cells. *Dyes and Pigments* **2017**, *146*, 136–142.

(35) Rosa, V.; Gaspari, A. P.; Folgosa, F.; Cordas, C. M.; Tavares, P.; Santos-Silva, T.; Barroso, S.; Aviles, T. Imine ligands based on ferrocene: synthesis, structural and Mössbauer characterization and evaluation as chromogenic and electrochemical sensors for Hg 2+. *New Journal of Chemistry* **2018**, *42*, 3334–3343.

(36) Dong, J.; Hu, J.; Baigude, H.; Zhang, H. A novel ferrocenyl–naphthalimide as a multichannel probe for the detection of Cu (II) and Hg (II) in aqueous media and living cells. *Dalton Transactions* **2018**, *47*, 314–322.

(37) Maity, A.; Sil, A.; Nad, S.; Patra, S. K. A highly selective, sensitive and reusable BODIPY based 'OFF/ON'fluorescence chemosensor for the detection of Hg2+ Ions. *Sensors and Actuators B: Chemical* **2018**, *255*, 299–308.

(38) Zhu, N.; Xu, J.; Ma, Q.; Geng, Y.; Li, L.; Liu, S.; Liu, S.; Wang, G. Rhodamine-based fluorescent probe for highly selective determination of Hg2+. *ACS omega* **2022**, *7*, 29236–29245.

(39) Guan, W.-L.; Zhang, Y.-F.; Zhang, Q.-P.; Zhang, Y.-M.; Wei, T.-B.; Yao, H.; Lin, Q. A novel fluorescent chemosensor based on naphthofuran functionalized naphthalimide for highly selective and sensitive detecting Hg2+ and CN-. *Journal of Luminescence* **2022**, *244*, 118722.

(40) Lee, C. G.; Kang, S.; Oh, J.; Eom, M. S.; Oh, J.; Kim, M.-G.; Lee, W. S.; Hong, S.; Han, M. S. A colorimetric and fluorescent chemosensor for detection of Hg2+ using

counterion exchange of cationic polydiacetylene. *Tetrahedron Letters* **2017**, *58*, 4340–4343.

(41) Rurack, K.; Resch-Genger, U.; Bricks, J. L.; Spieles, M. Cation-triggered 'switching on'of the red/near infra-red (NIR) fluorescence of rigid fluorophore–spacer–receptor ionophores. *Chemical communications* **2000**, 2103–2104.

(42) Rurack, K.; Kollmannsberger, M.; Resch-Genger, U.; Daub, J. A selective and sensitive fluoroionophore for HgII, AgI, and CuII with virtually decoupled fluorophore and receptor units. *Journal of the American Chemical Society* **2000**, *122*, 968–969.

(43) Kumar, A. Recent Development in Fluorescent Probes for the Detection of Hg2+ Ions. *Critical Reviews in Analytical Chemistry* **2023**, 1–44.

(44) Singh, I.; Kumar, G.; Palta, A.; Paul, K., et al. Naphthalimide-benzimidazole conjugate towards "Turn-on" recoginition of Hg2+ in pure aqueous medium. *Inorganica Chimica Acta* **2023**, *557*, 121684.

(45) Wu, X.-F.; Ma, Q.-J.; Wei, X.-J.; Hou, Y.-M.; Zhu, X. A selective fluorescent sensor for Hg2+ based on covalently immobilized naphthalimide derivative. *Sensors and Actuators B: Chemical* **2013**, *183*, 565–573.

(46) Un, H.-I.; Huang, C.-B.; Huang, C.; Jia, T.; Zhao, X.-L.; Wang, C.-H.; Xu, L.; Yang, H.-B. A versatile fluorescent dye based on naphthalimide: highly selective detection of Hg 2+ in aqueous solution and living cells and its aggregation-induced emission behaviour. *Organic Chemistry Frontiers* **2014**, *1*, 1083–1090.

(47) Zhang, Z.; Lu, S.; Sha, C.; Xu, D. A single thiourea-appended 1, 8-naphthalimide chemosensor for three heavy metal ions: Fe3+, Pb2+, and Hg2+. *Sensors and Actuators B: Chemical* **2015**, *208*, 258–266.

(48) Thapa, P.; Arnquist, I.; Byrnes, N.; Denisenko, A.; Foss Jr, F.; Jones, B.; McDonald, A. D.; Nygren, D. R.; Woodruff, K. Barium chemosensors with dry-phase fluorescence for neutrinoless double beta decay. *Scientific reports* **2019**, *9*, 15097.

(49) Rivilla, I.; Aparicio, B.; Bueno, J. M.; Casanova, D.; Tonnelé, C.; Freixa, Z.; Herrero, P.; Rogero, C.; Miranda, J. I.; Martínez-Ojeda, R. M., et al. Fluorescent bicolour sensor for low-background neutrinoless double β decay experiments. *Nature* **2020**, *583*, 48–54.

(50) Jones, B.; McDonald, A.; Nygren, D. Single molecule fluorescence imaging as a technique for barium tagging in neutrinoless double beta decay. *Journal of Instrumentation* **2016**, *11*, P12011.

(51) Herrero-Gómez, P.; Calupitan, J. P.; Ilyn, M.; Berdonces-Layunta, A.; Wang, T.; de Oteyza, D.; Corso, M.; González-Moreno, R.; Rivilla, I.; Aparicio, B., et al. Ba+ 2 ion trapping using organic submonolayer for ultra-low background neutrinoless double beta detector. *Nature Communications* **2022**, *13*, 7741.

(52) Navarro, K.; Jones, B.; Baeza-Rubio, J.; Boyd, M.; Denisenko, A.; Foss, F.; Giri, S.; Miller, R.; Nygren, D.; Tiscareno, M., et al. A Compact Dication Source for Ba^{2+} Tagging and Heavy Metal Ion Sensor Development. *arXiv preprint arXiv:2303.01522* **2023**,

(53) Corsaro, G. Ion strength, ion association, and solubility. *Journal of Chemical Education* **1962**, *39*, 622.

(54) Aghaie, M.; Aghaie, H.; Ebrahimi, A. Thermodynamics of the solubility of barium nitrate in the mixed solvent, ethanol+ water, and the related ion-association. *Journal of molecular liquids* **2007**, *135*, 72–74.

(55) Kalugin, O.; Agieienko, V.; Otroshko, N.; Moroz, V. Ionic association and solvation in solutions of magnesium and nickel perchlorates in acetonitrile. *Russian Journal of Physical Chemistry A* **2009**, *83*, 231–237.

(56) Linhart, G. On the association of mercuric chloride in water solution. *Journal of the American Chemical Society* **1915**, *37*, 258–274.

(57) Park, C. M.; Katz, L. E.; Liljestrand, H. M. Mercury speciation during in situ thermal desorption in soil. *Journal of Hazardous Materials* **2015**, *300*, 624–632.

(58) Deng, H.; Li, H. Specific cation effects on surface reactions of HgCl2 in clay-water systems. *Applied Clay Science* **2022**, *224*, 106523.

(59) DeRose, P. C.; Resch-Genger, U. Recommendations for fluorescence instrument qualification: the new ASTM Standard Guide. *Analytical chemistry* **2010**, *82*, 2129–2133.

(60) Irwin, K. D.; Hilton, G. C. Transition-edge sensors. *Cryogenic particle detection* **2005**, 63–150.

(61) Goldie, D.; Audley, M.; Glowacka, D.; Tsaneva, V.; Withington, S. Transition edge sensors for bolometric applications: responsivity and saturation. *Journal of Applied Physics* **2008**, *103*.

(62) Frisch, M. J. gaussian09. *http://www. gaussian. com/* **2009**,

(63) Hall, R. J.; Davidson, M. M.; Burton, N. A.; Hillier, I. H. Combined density functional, self-consistent reaction field model of solvation. *The Journal of Physical Chemistry* **1995**, *99*, 921–924.

(64) Zhao, Y.; Truhlar, D. G. The M06 suite of density functionals for main group thermochemistry, thermochemical kinetics, noncovalent interactions, excited states, and transition elements: two new functionals and systematic testing of four M06-class functionals and 12 other functionals. *Theoretical chemistry accounts* **2008**, *120*, 215–241.

(65) Weigend, F.; Ahlrichs, R. Balanced basis sets of split valence, triple zeta valence and quadruple zeta valence quality for H to Rn: Design and assessment of accuracy. *Physical Chemistry Chemical Physics* **2005**, *7*, 3297–3305.

(66) Weigend, F. Accurate Coulomb-fitting basis sets for H to Rn. *Physical chemistry chemical physics* **2006**, *8*, 1057–1065.